

Conditioning of a Hybrid High-Order scheme on meshes with small faces

Santiago Badia¹, Jérôme Droniou², and Liam Yemm³

¹School of Mathematics, Monash University, Clayton, Victoria, 3800, Australia & Centre Internacional de Mètodes Numèrics a l'Enginyeria, Barcelona, Spain santiago.badia@monash.edu

²School of Mathematics, Monash University, Clayton, Victoria, 3800, Australia, jerome.droniou@monash.edu

³School of Mathematics, Monash University, Clayton, Victoria, 3800, Australia, liam.yemm@monash.edu

Abstract

We conduct a condition number analysis of a Hybrid High-Order (HHO) scheme for the Poisson problem. We find the condition number of the statically condensed system to be independent of the number of faces in each element, or the relative size between an element and its faces. The dependence of the condition number on the polynomial degree is tracked. Next, we consider HHO schemes on cut background meshes, which are commonly used in unfitted discretisations. It is well known that the linear systems obtained on these meshes can be arbitrarily ill-conditioned due to the presence of sliver-cut and small-cut elements. We show that the condition number arising from HHO schemes on such meshes is not as negatively effected as those arising from conforming methods. We describe how the condition number can be improved by aggregating ill-conditioned elements with their neighbours.

Key words: Hybrid High-Order methods, condition number, small faces.

MSC2010: 65N12, 65N15, 65N30.

1 Introduction

Several hybrid discretisation methods have been proposed in recent years for the numerical discretisation of partial differential equations [20, 6, 16]. One of the selling points of these schemes is their geometrical flexibility. Discretisation spaces are not bound to specific element topologies and can readily be used on general polytopal meshes. Body-fitted unstructured mesh generation is one of the main bottlenecks in complex numerical simulations, which requires intensive human intervention. Usually, these meshes are composed of tetrahedral (and/or hexahedral) elements. Polytopal methods can provide sought-after flexibility in the mesh generation step.

In this work, we focus on the hybrid high-order (HHO) method. Developed in [20, 19], the HHO method is a modern polytopal method for elliptic PDEs. A key aspect of HHO is its applicability to generic meshes with arbitrarily shaped elements. Additionally, HHO methods are of arbitrary order, dimension independent, and are amenable to static condensation. We refer the reader to [18] for a thorough review of the method and its applications. An analysis on skewed meshes has been carried out for a diffusion problem in [22] and identifies how the error estimate is impacted by the element distortion and local diffusion tensor. The recent work of [23] shows the HHO method to be accurate on meshes possessing elements with arbitrarily many small faces.

Unfitted (a.k.a. embedded and immersed) discretisations can also simplify the geometrical discretisation step. The domain of interest is embedded in a simple background mesh (e.g., a

Cartesian grid). The boundary (or interface) treatment is tackled at the numerical integration and discretisation step. Many unfitted finite element (FE) schemes that rely on a standard FE space on the background mesh have been proposed; see, e.g. the extended finite element method (XFEM) [8], the cutFEM method [11], the aggregated finite element method (FEM) [5], the finite cell method [29] and discontinuous Galerkin (DG) methods with element aggregation [26]. We also make note of the reference [7], which uses a virtual element method (VEM) to model a rigid leaflet submerged in a fluid and fixed to a rotational spring at one end. The thin leaflet ‘cuts’ through an isotropic background mesh, thus requiring the model to be applied on cut meshes.

Unfitted formulations can produce arbitrarily ill-conditioned linear systems [17]. The intersection of a background element with the physical domain can be arbitrarily small and with an unbounded aspect ratio. It is known as the *small cut element problem*. This problem is also present on unfitted interfaces with a high contrast of physical properties [28]. Few unfitted formulations are fully robust and optimal regardless of cut location or material contrast. The ill-conditioning issue was addressed in [9] via the so-called ghost penalty stabilisation. Instead of adding stabilisation terms, the small cut element problem can be fixed by element aggregation (or agglomeration). This approach has been proposed in [26] for DG methods. While aggregation is natural in DG methods (these schemes can readily be used on polytopal meshes), its extension to conforming spaces is more involved. The design of well-posed \mathcal{C}^0 Lagrangian finite elements on agglomerated meshes has been proposed in [5]. The aggregated FEM constructs a discrete extension operator from well-posed to ill-posed degrees of freedom that preserves continuity. All these formulations enjoy good numerical properties, such as stability, condition number bounds, optimal convergence and continuity with respect to data.

The FE discretisation of linear second-order elliptic operators (e.g. the Laplacian) in weak form produces linear systems such that the ℓ^2 -condition number (on shape regular, quasi-uniform meshes) scales as the inverse square of the mesh size [24]. Likewise, the condition number on regular triangular meshes of interior penalty Galerkin and local discontinuous Galerkin methods scale as the inverse square of the mesh size, whereas the condition number of non-symmetric DG methods can potentially scale sub-optimally [13]. We refer to [15] for the condition number analysis of hybridizable discontinuous Galerkin (HDG) methods on regular simplicial quasi-uniform meshes. The authors in [27] investigate experimentally the ill-conditioning of the VEM for high-order bases on distorted meshes. In this work, we analyse the properties of the linear systems that arise from HHO formulations. We prove estimates for the condition number arising from such systems. Under general assumptions on the stabilisation term (allowing for standard choices of HHO stabilisation) and when L^2 -orthonormal bases are chosen for face polynomial spaces, we show that the estimates remain robust with respect to small element faces and track the dependence in the estimates of the polynomial degree of the unknowns. The linear systems in HHO methods are obtained after the static condensation of the element unknowns. This process allows the global system to depend only on the face unknowns [18, Appendix B.3.2]. In Section 2.2.3 we state some estimates on the spectrum and conditioning of this condensed operator. We find that the condition number of the statically condensed system scales at worst like h_{\min}^{-2} (where h_{\min} denotes the minimum element diameter in the mesh) and that this bound is not affected by small faces. We also prove that if each face is attached (or close) to at least one element of diameter comparable to a characteristic mesh size h_{\max} , then the condition number scales as $h_{\min}^{-1} h_{\max}^{-1}$. This sharper result is of practical interest when using cut meshes, since it is common to find small cells on the boundary in touch with larger ones. To the best of our knowledge, no condition number estimates on general meshes exist for HHO or VEM. We note that, given the links between HHO and other polytopal methods (see e.g. [18, Sec. 5.5.5] for the relationship between HHO and non-conforming VEM, or [14] for the link HHO–HDG), our results could easily

be extended to such methods; more generally, the analysis of condition number we carry out here uses a rather general approach and would certainly extend to even more polytopal methods.

Next, we apply the HHO method on *cut* meshes obtained by the intersection of cells in a background (usually Cartesian) mesh and the physical domain (represented as the interior of an oriented boundary representation, e.g., a surface mesh). The intersection is cell-wise and represents a sound alternative to unstructured mesh generation [2]. The analysis tells us the potential conditioning issues of HHO schemes on such meshes, for which arbitrarily small elements (and faces) appear scattered among large elements [10]. Based on the analysis, we know that we must aggregate highly distorted small cut elements (e.g., due to sliver cuts) to interior elements. Since arbitrary small faces do not affect condition number bounds, there is no need for face aggregation or stabilisation. This way, we end up with an HHO method on aggregated cut meshes that leads to well-posed linear systems and optimal condition numbers.

Hybrid methods on cut meshes have some benefits compared to more standard unfitted FEs. First, we can enforce Dirichlet boundary conditions strongly; there are degrees of freedom located on boundaries faces. In unfitted standard FEs, degrees of freedom are defined in the background mesh. Dirichlet boundary conditions and trace continuity on interfaces are weakly enforced (using, e.g., Nitsche's method [25]). Second, the method does not involve the tuning of additional stabilisation parameters, which can have an impact on results [3]. Third, the extension to high order is straightforward. It is more complicated in face-based ghost penalty (it involves penalty terms on jumps of high-order derivatives) [9] or aggregated FEs (extension operators for high order can amplify rounding errors) [5].

The remainder of this paper is organised as follows: In Section 2 we introduce the HHO method and state our key findings. In Section 3 we prove the results and discuss viable stabilisation options, in Section 4 we include a brief discussion of HHO on cut meshes, and in Section 5 we conduct a thorough numerical study of the condition number on various meshes.

2 Presentation of the HHO method and main result

2.1 Model problem

We take a polytopal domain $\Omega \subset \mathbb{R}^d$, $d \geq 2$ and a source term $f \in L^2(\Omega)$, and consider the Dirichlet problem: find u such that

$$\begin{aligned} -\Delta u &= f & \text{in } \Omega, \\ u &= 0 & \text{on } \partial\Omega. \end{aligned}$$

The variational problem reads: find $u \in H_0^1(\Omega)$ such that

$$a(u, v) = \mathcal{L}(v), \quad \forall v \in H_0^1(\Omega), \quad (2.1)$$

where $a(u, v) := (\nabla u, \nabla v)_\Omega$ and $\mathcal{L}(v) := (f, v)_\Omega$. Here and in the following, $(\cdot, \cdot)_X$ is the L^2 -inner product of scalar- or vector-valued functions on a set X for its natural measure.

2.2 HHO scheme

Let $\mathcal{H} \subset (0, \infty)$ be a countable set of mesh sizes with a unique cluster point at 0. For each $h \in \mathcal{H}$, we partition the domain Ω into a mesh $\mathcal{M}_h = (\mathcal{T}_h, \mathcal{F}_h)$, for which a detailed definition can be found in [18, Definition 1.4]. The set of mesh elements \mathcal{T}_h is a disjoint set of polytopes such that $\overline{\Omega} = \bigcup_{T \in \mathcal{T}_h} \overline{T}$. The set \mathcal{F}_h is a collection of mesh faces forming a partition of the mesh

skeleton, i.e. $\bigcup_{T \in \mathcal{T}_h} \partial T = \bigcup_{F \in \mathcal{F}_h} \overline{F}$. The boundary faces $F \subset \partial\Omega$ are gathered in the set \mathcal{F}_h^b . The parameter h is given by $h := \max_{T \in \mathcal{T}_h} h_T$ where, for $X = T \in \mathcal{T}_h$ or $X = F \in \mathcal{F}_h$, h_X denotes the diameter of X . We shall also collect the set of faces attached to an element $T \in \mathcal{T}_h$ in the set $\mathcal{F}_T := \{F \in \mathcal{F}_h : F \subset T\}$. The (constant) unit normal to $F \in \mathcal{F}_T$ pointing outside T is denoted by \mathbf{n}_{TF} , and $\mathbf{n}_{\partial T} : \partial T \rightarrow \mathbb{R}^d$ is the piecewise constant outer unit normal defined by $(\mathbf{n}_{\partial T})|_F = \mathbf{n}_{TF}$ for all $F \in \mathcal{F}_T$. Throughout this work we make the following assumption on the meshes, which allows for some meshes with arbitrarily large numbers of face in each element, or faces that have an arbitrarily small diameter compared to their elements' diameters.

Assumption 1 (Regular mesh sequence). *There exists a constant $\varrho > 0$ such that, for each $h \in \mathcal{H}$, each $T \in \mathcal{T}_h$ is connected by star-shaped sets with parameter ϱ , as defined in [18, Definition 1.41].*

From hereon, we shall denote $f \lesssim g$ to mean $f \leq Cg$ where C is a constant depending only on Ω , d and ϱ , but independent of the considered face/element, the degrees of the considered polynomial spaces, and quantities f, g . We shall also write $f \approx g$ if $f \lesssim g$ and $g \lesssim f$. When necessary, we make some additional dependencies of the constant C explicit.

2.2.1 Local construction

Let $X = T \in \mathcal{T}_h$ or $X = F \in \mathcal{F}_h$ be a face or an element in a mesh \mathcal{M}_h , and let $\mathbb{P}^\ell(X)$ be the set of d_X -variate polynomials of degree $\leq \ell$ on X , where d_X is the dimension of X . The space of piecewise discontinuous polynomial functions on an element boundary is given by

$$\mathbb{P}^\ell(\mathcal{F}_T) := \{v \in L^1(\partial T) : v|_F \in \mathbb{P}^\ell(F) \quad \forall F \in \mathcal{F}_T\}. \quad (2.2)$$

The L^2 orthogonal projector $\pi_X^{0,\ell} : L^1(X) \rightarrow \mathbb{P}^\ell(X)$ is defined as the unique polynomial satisfying

$$(v - \pi_X^{0,\ell} v, w)_X = 0 \quad \forall w \in \mathbb{P}^\ell(X). \quad (2.3)$$

Fix two natural numbers $k, l \in \mathbb{N}$, $l \geq k - 1$. For each element $T \in \mathcal{T}_h$, the local space of unknowns is defined as

$$\underline{U}_T^{k,l} := \mathbb{P}^l(T) \times \mathbb{P}^k(\mathcal{F}_T).$$

The interpolator $\underline{I}_T^{k,l} : H^1(T) \rightarrow \underline{U}_T^{k,l}$ is defined for all $v \in H^1(T)$ as

$$\underline{I}_T^{k,l} v = (\pi_T^{0,l} v, \pi_{\partial T}^{0,k} v)$$

where $\pi_{\partial T}^{0,k}$ is the projector onto the space $\mathbb{P}^k(\mathcal{F}_T)$ satisfying $\pi_{\partial T}^{0,k} v|_F = \pi_F^{0,k} v$ for all $F \in \mathcal{F}_T$ and $v \in L^1(\partial T)$. We endow the space $\underline{U}_T^{k,l}$ with the discrete energy-like seminorm $\|\cdot\|_{1,T}$ defined for all $\underline{v}_T = (v_T, v_{\partial T}) \in \underline{U}_T^{k,l}$ via

$$\|\underline{v}_T\|_{1,T}^2 := \|\nabla v_T\|_T^2 + h_T^{-1} \|v_{\partial T} - v_T\|_{\partial T}^2. \quad (2.4)$$

On each element we locally reconstruct a potential from the space of unknowns via the operator $\mathbf{p}_T^{k+1} : \underline{U}_T^{k,l} \rightarrow \mathbb{P}^{k+1}(T)$ defined to satisfy, for all $\underline{v}_T \in \underline{U}_T^{k,l}$ and $w \in \mathbb{P}^{k+1}(T)$,

$$(\nabla \mathbf{p}_T^{k+1} \underline{v}_T, \nabla w)_T = -(v_T, \Delta w)_T + (v_{\partial T}, \nabla w \cdot \mathbf{n}_{\partial T})_{\partial T}, \quad (2.5)$$

$$(v_T - \mathbf{p}_T^{k+1} \underline{v}_T, 1)_T = 0. \quad (2.6)$$

This potential reconstruction allows us to approximate $a(u, v)$ on each element by the bilinear form $a_T : \underline{U}_T^{k,l} \times \underline{U}_T^{k,l} \rightarrow \mathbb{R}$ defined as

$$a_T(\underline{u}_T, \underline{v}_T) := (\nabla p_T^{k+1} \underline{u}_T, \nabla p_T^{k+1} \underline{v}_T)_T + s_T(\underline{u}_T, \underline{v}_T),$$

where $s_T : \underline{U}_T^{k,l} \times \underline{U}_T^{k,l} \rightarrow \mathbb{R}$ is a symmetric, positive semi-definite stabilisation such that

$$C_a^{-1} \|\underline{v}_T\|_{1,T}^2 \leq a_T(\underline{v}_T, \underline{v}_T) \leq C_a \|\underline{v}_T\|_{1,T}^2 \quad (2.7)$$

and for all $\underline{v}_T \in \underline{U}_T^{k,l}$, $w \in \mathbb{P}^{k+1}(T)$,

$$s_T(\underline{v}_T, \underline{I}_T^{k,l} w) = 0, \quad (2.8)$$

where C_a is a positive constant that possibly depends on polynomial degrees l , k , the mesh regularity ϱ , and dimension d , but is independent of the element diameter h_T . Equation (2.7) is required to ensure that the global bilinear form describes a norm on the discrete space, and that optimal approximation rates with respect to h are achieved [18, Lemma 2.18]. However, tracking the dependency of C_a with respect to l , k and obtaining condition number estimates via equation (2.7) leads to sub-optimal results. As such, we assume the following extra, more precise, conditions on the bilinear form s_T , in which the difference operators $\delta_T^l : \underline{U}_T^{k,l} \rightarrow \mathbb{P}^l(T)$ and $\delta_{\partial T}^k : \underline{U}_T^{k,l} \rightarrow \mathbb{P}^k(\mathcal{F}_T)$ are defined as: for all $\underline{v}_T \in \underline{U}_T^{k,l}$,

$$\delta_T^l \underline{v}_T := \pi_T^{0,l}(p_T^{k+1} \underline{v}_T - v_T) \quad \text{and} \quad \delta_{\partial T}^k \underline{v}_T := \pi_{\partial T}^{0,k}(p_T^{k+1} \underline{v}_T - v_{\partial T}).$$

Assumption 2. For all $\underline{v}_T \in \underline{U}_T^{k,l}$ it holds that

$$\|\nabla p_T^{k+1} \underline{v}_T\|_T^2 + h_T^{-1} \|\delta_{\partial T}^k \underline{v}_T\|_{\partial T}^2 \lesssim a_T(\underline{v}_T, \underline{v}_T), \quad (2.9)$$

and for all $\underline{v}_{T,\partial} = (0, v_{\partial T}) \in \underline{U}_T^{k,l}$ it holds that

$$a_T(\underline{v}_{T,\partial}, \underline{v}_{T,\partial}) \lesssim \|\nabla p_T^{k+1} \underline{v}_{T,\partial}\|_T^2 + h_T^{-1} \|\delta_{\partial T}^k \underline{v}_{T,\partial}\|_{\partial T}^2, \quad (2.10)$$

where the hidden constants in (2.9) and (2.10) depend on ϱ and d but are independent of l , k and h .

We consider throughout this work the stabilisation form defined in [18, Example 2.8] (with the scaling change $h_F^{-1} \rightarrow h_T^{-1}$)

$$s_T(\underline{u}_T, \underline{v}_T) := h_T^{-2} (\delta_T^l \underline{u}_T, \delta_T^l \underline{v}_T)_T + h_T^{-1} (\delta_{\partial T}^k \underline{u}_T, \delta_{\partial T}^k \underline{v}_T)_{\partial T}. \quad (2.11)$$

We show in Section 3.2 that the stabilisation (2.11) satisfies Assumption 2.

2.2.2 Global formulation

The global space of unknowns is defined as

$$\underline{U}_h^{k,l} := \left\{ \underline{v}_h = ((v_T)_{T \in \mathcal{T}_h}, (v_F)_{F \in \mathcal{F}_h}) : v_T \in \mathbb{P}^l(T) \quad \forall T \in \mathcal{T}_h, v_F \in \mathbb{P}^k(F) \quad \forall F \in \mathcal{F}_h \right\}.$$

To account for the homogeneous boundary conditions, the following subspace is also introduced:

$$\underline{U}_{h,0}^{k,l} := \{ \underline{v}_h \in \underline{U}_h^{k,l} : v_F = 0 \quad \forall F \in \mathcal{F}_h^b \}.$$

For any $\underline{v}_h \in \underline{U}_h^{k,l}$ we denote its restriction to an element T by $\underline{v}_T = (v_T, v_{\partial T}) \in \underline{U}_T^{k,l}$ (where, naturally, $v_{\partial T}$ is defined from $(v_F)_{F \in \mathcal{F}_T}$). We also denote by v_h the piecewise polynomial function satisfying $v_h|_T = v_T$ for all $T \in \mathcal{T}_h$.

The global bilinear forms $\mathbf{a}_h : \underline{U}_h^{k,l} \times \underline{U}_h^{k,l} \rightarrow \mathbb{R}$ and $\mathbf{s}_h : \underline{U}_h^{k,l} \times \underline{U}_h^{k,l} \rightarrow \mathbb{R}$ are defined as

$$\mathbf{a}_h(\underline{u}_h, \underline{v}_h) := \sum_{T \in \mathcal{T}_h} \mathbf{a}_T(\underline{u}_T, \underline{v}_T) \quad \text{and} \quad \mathbf{s}_h(\underline{u}_h, \underline{v}_h) := \sum_{T \in \mathcal{T}_h} \mathbf{s}_T(\underline{u}_T, \underline{v}_T).$$

We also define the discrete energy norm $\|\cdot\|_{\mathbf{a},h}$ on $\underline{U}_{h,0}^{k,l}$ as

$$\|\underline{v}_h\|_{\mathbf{a},h} := \mathbf{a}_h(\underline{v}_h, \underline{v}_h)^{\frac{1}{2}} \quad \forall \underline{v}_h \in \underline{U}_{h,0}^{k,l}. \quad (2.12)$$

The HHO scheme reads: find $\underline{u}_h \in \underline{U}_{h,0}^{k,l}$ such that

$$\mathbf{a}_h(\underline{u}_h, \underline{v}_h) = \mathcal{L}_h(\underline{v}_h) \quad \forall \underline{v}_h \in \underline{U}_{h,0}^{k,l}, \quad (2.13)$$

where $\mathcal{L}_h : \underline{U}_{h,0}^{k,l} \rightarrow \mathbb{R}$ is a linear form defined as

$$\mathcal{L}_h(\underline{v}_h) := \sum_{T \in \mathcal{T}_h} (f, v_T)_T.$$

Under assumptions (2.7) and (2.8) on the bilinear form \mathbf{a}_T , the scheme (2.13) satisfies the energy error estimate

$$\|\underline{u}_h - \underline{I}_h^{k,l} u\|_{\mathbf{a},h} \leq C h^{k+1} |u|_{H^{k+2}(\mathcal{T}_h)},$$

where $\underline{I}_h^{k,l}|_T = \underline{I}_T^{k,l}$ for all $T \in \mathcal{T}_h$, and C is a positive constant that depends on l, k, ϱ , and d , but is independent of h [18, Theorem 2.27]. An estimate of the dependency with respect to l and k for a diffusion scheme with a boundary based stabilisation is provided in [1].

2.2.3 Statically condensed system and eigenvalue estimates

The static condensation procedure, as outlined in [18, Appendix B.3], allows for the elimination of the element unknowns. Selecting \underline{v}_h with one free element component v_T , and all other element and face components vanishing, we see that the solution \underline{u}_h to problem (2.13) satisfies for all $T \in \mathcal{T}_h$ and $v_T \in \mathbb{P}^l(T)$

$$\mathbf{a}_T((u_T, u_{\partial T}), (v_T, 0)) = (f, v_T)_T.$$

This can be alternatively written as

$$\mathbf{a}_T((u_T, 0), (v_T, 0)) = (f, v_T)_T - \mathbf{a}_T((0, u_{\partial T}), (v_T, 0)).$$

Noting that the bilinear form $(u_T, v_T) \in \mathbb{P}^k(T) \times \mathbb{P}^k(T) \mapsto \mathbf{a}_T((u_T, 0), (v_T, 0))$ is coercive (due to (2.7)), we can define the polynomial $g_T \in \mathbb{P}^l(T)$ and the linear operator $\mathcal{S}_T : \mathbb{P}^k(\mathcal{F}_T) \rightarrow \mathbb{P}^l(T)$ via

$$\mathbf{a}_T((g_T, 0), (v_T, 0)) = (f, v_T)_T \quad \forall v_T \in \mathbb{P}^l(T), \quad (2.14)$$

$$\mathbf{a}_T((\mathcal{S}_T u_{\partial T}, 0), (v_T, 0)) = -\mathbf{a}_T((0, u_{\partial T}), (v_T, 0)) \quad \forall v_T \in \mathbb{P}^l(T). \quad (2.15)$$

Therefore, u_T is calculated from $u_{\partial T}$ via the affine transformation

$$u_T = \mathcal{S}_T u_{\partial T} + g_T. \quad (2.16)$$

Substituting (2.16) into (2.13) and testing against $\underline{v}_h = (0, v_{\mathcal{F}_h}) = ((0)_{T \in \mathcal{T}_h}, (v_F)_{F \in \mathcal{F}_h}) \in \underline{U}_{-h,0}^{k,l}$ yields

$$\sum_{T \in \mathcal{T}_h} a_T((\mathcal{S}_T u_{\partial T}, u_{\partial T}), (0, v_{\partial T})) + \sum_{T \in \mathcal{T}_h} a_T((g_T, 0), (0, v_{\partial T})) = 0.$$

Setting

$$\mathbb{P}_0^k(\mathcal{F}_h) := \{u_{\mathcal{F}_h} = (u_F)_{F \in \mathcal{F}_h} : u_F \in \mathbb{P}^k(F) \quad \forall F \in \mathcal{F}_h, \quad u_F = 0 \text{ if } F \subset \partial\Omega\},$$

the statically condensed problem then reads: find $u_{\mathcal{F}_h} \in \mathbb{P}_0^k(\mathcal{F}_h)$ such that

$$\mathbf{A}_h(u_{\mathcal{F}_h}, v_{\mathcal{F}_h}) = \mathbf{L}_h(v_{\mathcal{F}_h}) \quad \forall v_{\mathcal{F}_h} \in \mathbb{P}_0^k(\mathcal{F}_h), \quad (2.17)$$

where

$$\begin{aligned} \mathbf{A}_h(u_{\mathcal{F}_h}, v_{\mathcal{F}_h}) &:= \sum_{T \in \mathcal{T}_h} a_T((\mathcal{S}_T u_{\partial T}, u_{\partial T}), (0, v_{\partial T})), \\ \mathbf{L}_h(v_{\mathcal{F}_h}) &:= \sum_{T \in \mathcal{T}_h} -a_T((g_T, 0), (0, v_{\partial T})). \end{aligned} \quad (2.18)$$

Upon choosing bases of the spaces $\mathbb{P}^k(F)$ for $F \in \mathcal{F}_h^i$, (2.17) takes the equivalent algebraic form

$$\mathbf{A}_h \mathbf{U} = \mathbf{F}$$

where \mathbf{A}_h is the matrix of the bilinear form \mathbf{A}_h , \mathbf{U} the vector of unknowns and \mathbf{F} the source term corresponding to \mathbf{L}_h . Our main result is the following; its proof is given in Section 3.1.

Theorem 1 (Eigenvalue and condition number estimates). *For each $F \in \mathcal{F}_h^i$, denote by T_F^+, T_F^- the two elements on each side of F , and define the characteristic lengths $H_{\mathcal{F}_h, \min}$ and $H_{\mathcal{F}_h, \max}$ by*

$$H_{\mathcal{F}_h, \min} = \min_{F \in \mathcal{F}_h} (h_{T_F^+} + h_{T_F^-}), \quad H_{\mathcal{F}_h, \max}^{-1} = \max_{F \in \mathcal{F}_h} (h_{T_F^+}^{-1} + h_{T_F^-}^{-1}).$$

If, for each $F \in \mathcal{F}_h^i$, the basis on $\mathbb{P}^k(F)$ is orthonormal for the $L^2(F)$ -inner product, then the minimal eigenvalue, maximal eigenvalue and condition number of \mathbf{A}_h satisfy

$$\lambda_{\min}(\mathbf{A}_h) \gtrsim H_{\mathcal{F}_h, \min}, \quad (2.19a)$$

$$\lambda_{\max}(\mathbf{A}_h) \lesssim (k+1)^2 H_{\mathcal{F}_h, \max}^{-1}, \quad (2.19b)$$

$$\kappa(\mathbf{A}_h) \lesssim (k+1)^2 H_{\mathcal{F}_h, \max}^{-1} H_{\mathcal{F}_h, \min}^{-1}. \quad (2.19c)$$

Remark 1 (Characteristic lengths). *Setting $h_{\min} = \min_{T \in \mathcal{T}_h} h_T$, we have $H_{\mathcal{F}_h, \min} \gtrsim h_{\min}$ and $H_{\mathcal{F}_h, \max}^{-1} \lesssim h_{\min}^{-1}$. Hence, (2.19) leads to the bounds*

$$\lambda_{\min}(\mathbf{A}_h) \gtrsim h_{\min}, \quad \lambda_{\max}(\mathbf{A}_h) \lesssim (k+1)^2 h_{\min}^{-1}, \quad \kappa(\mathbf{A}_h) \lesssim (k+1)^2 h_{\min}^{-2}.$$

For quasi-uniform meshes, h_{\min} can be replaced above by h in these estimates. However, on specific meshes (especially cut meshes with small cut elements), (2.19) can lead to much better estimates than those purely based on h_{\min} ; see Section 5.

Note that the factor $(k+1)^2$ appearing in (2.19b) and (2.19c) is due to the dependency on the polynomial degree of the generic discrete trace inequality (3.2).

Remark 2 (Small faces). *The estimates (2.19) are fully independent of the maximum number of faces in each element, or on their diameter, and are therefore fully robust with respect to small faces.*

3 Proofs

3.1 Estimate on the eigenvalues

Let us start with two preliminary estimates. The proof of the following trace inequality, under Assumption 1 (and therefore with hidden constants in \lesssim that are not impacted by the presence of small faces in T), can be found in [12, Section 3].

Lemma 2 (Trace Inequality). *For all $v \in H^1(T)$,*

$$\|v\|_{\partial T}^2 \lesssim h_T^{-1} \left(\|v\|_T^2 + h_T^2 \|\nabla v\|_T^2 \right). \quad (3.1)$$

For $v \in \mathbb{P}^\ell(T)$, the following discrete trace inequality also holds:

$$\|v\|_{\partial T}^2 \lesssim h_T^{-1} (\ell + 1)(\ell + d) \|v\|_T^2. \quad (3.2)$$

Lemma 3 (Poincaré–Wirtinger). *For all $v \in H^1(T)$ the following Poincaré–Wirtinger inequality holds:*

$$\|v - \pi_T^{0,0} v\|_T \lesssim h_T |v|_{H^1(T)}. \quad (3.3)$$

Proof. See [18, Remark 1.46]. \square

Lemma 4 (Discrete Poincaré inequality). *For all $\underline{v}_h \in \underline{U}_{h,0}^{k,l}$ it holds that*

$$\sum_{T \in \mathcal{T}_h} h_T \|v_{\partial T}\|_{\partial T}^2 \lesssim \sum_{T \in \mathcal{T}_h} \left(\|\nabla \mathbf{p}_T^{k+1} \underline{v}_T\|_T^2 + h_T^{-1} \|\delta_{\partial T}^k \underline{v}_T\|_{\partial T}^2 \right), \quad (3.4)$$

where the hidden constant depends on d , ϱ and Ω but is independent of l , k and h .

Proof. By a triangle inequality it holds that

$$\sum_{T \in \mathcal{T}_h} h_T \|v_{\partial T}\|_{\partial T}^2 \lesssim \sum_{T \in \mathcal{T}_h} h_T \|\pi_{\partial T}^{0,k} \mathbf{p}_T^{k+1} \underline{v}_T\|_{\partial T}^2 + \sum_{T \in \mathcal{T}_h} h_T \|\delta_{\partial T}^k \underline{v}_T\|_{\partial T}^2.$$

The second term clearly satisfies the desired bound due to $h_T \leq \text{diam}(\Omega)^2 h_T^{-1}$. It holds by the boundedness of $\pi_{\partial T}^{0,k} \mathbf{p}_T^{k+1} \underline{v}_T$ and the continuous trace inequality (3.1) that

$$\sum_{T \in \mathcal{T}_h} h_T \|\pi_{\partial T}^{0,k} \mathbf{p}_T^{k+1} \underline{v}_T\|_{\partial T}^2 \lesssim \sum_{T \in \mathcal{T}_h} \left(\|\mathbf{p}_T^{k+1} \underline{v}_T\|_T^2 + h_T^2 \|\nabla \mathbf{p}_T^{k+1} \underline{v}_T\|_T^2 \right).$$

Thus it remains to prove that

$$\|\mathbf{p}_h^{k+1} \underline{v}_h\|_\Omega^2 \lesssim \sum_{T \in \mathcal{T}_h} \left(\|\nabla \mathbf{p}_T^{k+1} \underline{v}_T\|_T^2 + h_T^{-1} \|\delta_{\partial T}^k \underline{v}_T\|_{\partial T}^2 \right).$$

As the divergence operator $\nabla \cdot : H^1(\Omega)^d \rightarrow L^2(\Omega)$ is onto, there exists a $\boldsymbol{\tau} \in H^1(\Omega)^d$ such that $-\nabla \cdot \boldsymbol{\tau} = \mathbf{p}_h^{k+1} \underline{v}_h$ and $\|\boldsymbol{\tau}\|_{H^1(\Omega)^d} \lesssim \|\mathbf{p}_h^{k+1} \underline{v}_h\|_\Omega$ [18, Lemma 8.3]. Therefore

$$\begin{aligned} \|\mathbf{p}_h^{k+1} \underline{v}_h\|_\Omega^2 &= -(\mathbf{p}_h^{k+1} \underline{v}_h, \nabla \cdot \boldsymbol{\tau})_\Omega = \sum_{T \in \mathcal{T}_h} \left((\nabla \mathbf{p}_T^{k+1} \underline{v}_T, \boldsymbol{\tau})_T - (\mathbf{p}_T^{k+1} \underline{v}_T, \boldsymbol{\tau} \cdot \mathbf{n}_{\partial T})_{\partial T} \right) \\ &= \sum_{T \in \mathcal{T}_h} \left((\nabla \mathbf{p}_T^{k+1} \underline{v}_T, \boldsymbol{\tau})_T + (v_{\partial T} - \mathbf{p}_T^{k+1} \underline{v}_T, \boldsymbol{\tau} \cdot \mathbf{n}_{\partial T})_{\partial T} \right), \end{aligned}$$

where we have invoked the homogeneous conditions on the space $\underline{U}_{h,0}^{k,l}$ and the fact that $\boldsymbol{\tau} \cdot \mathbf{n}_{TF} + \boldsymbol{\tau} \cdot \mathbf{n}_{T'F} = 0$ whenever T, T' are the two elements on each side of an internal face $F \in \mathcal{F}_h^i$. Thus, by the Cauchy–Schwarz inequality and continuous trace inequalities it holds that

$$\begin{aligned} \|\mathbf{p}_h^{k+1} \underline{v}_h\|_\Omega^2 &\lesssim \sum_{T \in \mathcal{T}_h} \|\boldsymbol{\tau}\|_{H^1(T)} \left(\|\nabla \mathbf{p}_T^{k+1} \underline{v}_T\|_T + h_T^{-\frac{1}{2}} \|v_{\partial T} - \mathbf{p}_T^{k+1} \underline{v}_T\|_{\partial T} \right) \\ &\lesssim \sum_{T \in \mathcal{T}_h} \|\boldsymbol{\tau}\|_{H^1(T)} \left(\|\nabla \mathbf{p}_T^{k+1} \underline{v}_T\|_T + h_T^{-\frac{1}{2}} \|\delta_{\partial T}^k \underline{v}_T\|_{\partial T} \right), \end{aligned}$$

where in the second line we have added and subtracted $\pi_{\partial T}^{0,k} \mathbf{p}_T^{k+1} \underline{v}_T$ to the boundary term, invoked the minimisation of $\pi_{\partial T}^{0,k}$ and applied a continuous trace inequality. The proof follows from a discrete Cauchy–Schwarz inequality and the bound $\|\boldsymbol{\tau}\|_{H^1(\Omega)^d} \lesssim \|\mathbf{p}_h^{k+1} \underline{v}_h\|_\Omega$. \square

Lemma 5. *For all $\underline{v}_{T,\partial} = (0, v_{\partial T}) \in \underline{U}_T^{k,l}$, it holds that*

$$\|\nabla \mathbf{p}_T^{k+1} \underline{v}_{T,\partial}\|_T^2 + h_T^{-1} \|\delta_{\partial T}^k \underline{v}_{T,\partial}\|_{\partial T}^2 \lesssim (k+1)^2 h_T^{-1} \|v_{\partial T}\|_{\partial T}^2, \quad (3.5)$$

where the hidden constant depends on d and ϱ but is independent of l , k and h .

Proof. By a triangle inequality, the boundedness of $\pi_{\partial T}^{0,k}$, and the continuous trace inequality (3.1) it holds that

$$h_T^{-1} \|\delta_{\partial T}^k \underline{v}_{T,\partial}\|_{\partial T}^2 \lesssim h_T^{-1} \|v_{\partial T}\|_{\partial T}^2 + h_T^{-2} \|\mathbf{p}_T^{k+1} \underline{v}_{T,\partial}\|_T^2 + \|\nabla \mathbf{p}_T^{k+1} \underline{v}_{T,\partial}\|_T^2.$$

As the element unknown is zero, it holds by (2.6) that $\pi_T^{0,0} \mathbf{p}_T^{k+1} \underline{v}_{T,\partial} = 0$. Thus, we may apply Poincaré–Wirtinger inequality (3.3) to yield $h_T^{-2} \|\mathbf{p}_T^{k+1} \underline{v}_{T,\partial}\|_T^2 \lesssim \|\nabla \mathbf{p}_T^{k+1} \underline{v}_{T,\partial}\|_T^2$. Hence, it remains to be proven that

$$\|\nabla \mathbf{p}_T^{k+1} \underline{v}_{T,\partial}\|_T^2 \lesssim (k+1)^2 h_T^{-1} \|v_{\partial T}\|_{\partial T}^2. \quad (3.6)$$

It follows from equation (2.5) with $w = \mathbf{p}_T^{k+1} \underline{v}_{T,\partial}$ that

$$\|\nabla \mathbf{p}_T^{k+1} \underline{v}_{T,\partial}\|_T^2 = (v_{\partial T}, \nabla \mathbf{p}_T^{k+1} \underline{v}_{T,\partial} \cdot \mathbf{n}_{\partial T})_{\partial T}.$$

Applying the discrete trace inequality (3.2) and $(k+1)(k+d) \lesssim (k+1)^2$ yields

$$\|\nabla \mathbf{p}_T^{k+1} \underline{v}_{T,\partial}\|_T^2 \lesssim h_T^{-\frac{1}{2}} (k+1) \|v_{\partial T}\|_{\partial T} \|\nabla \mathbf{p}_T^{k+1} \underline{v}_{T,\partial}\|_T.$$

Simplifying by $\|\nabla \mathbf{p}_T^{k+1} \underline{v}_{T,\partial}\|_T$ and squaring yields the desired result (3.6). \square

We can now prove the estimates (2.19) on the eigenvalues and condition number of \mathbf{A}_h .

Proof of Theorem 1. We note that

$$\mathbf{a}_T((\mathcal{S}_T u_{\partial T}, u_{\partial T}), (0, u_{\partial T})) = \mathbf{a}_T((\mathcal{S}_T u_{\partial T}, u_{\partial T}), (\mathcal{S}_T u_{\partial T}, u_{\partial T})) - \cancel{\mathbf{a}_T((\mathcal{S}_T u_{\partial T}, u_{\partial T}), (\mathcal{S}_T u_{\partial T}, 0))}$$

where the cancellation follows setting $v_T = \mathcal{S}_T u_{\partial T}$ in (2.15). By equations (3.4) and (2.9), and recalling the definition (2.18) of \mathbf{A}_h , it thus holds that

$$\sum_{T \in \mathcal{T}_h} h_T \|u_{\partial T}\|_{\partial T}^2 \lesssim \mathbf{A}_h(u_{\mathcal{F}_h}, u_{\mathcal{F}_h}). \quad (3.7)$$

Consider also

$$\begin{aligned} \mathbf{a}_T((\mathcal{S}_T u_{\partial T}, u_{\partial T}), (0, u_{\partial T})) &= \mathbf{a}_T((0, u_{\partial T}), (0, u_{\partial T})) + \mathbf{a}_T((\mathcal{S}_T u_{\partial T}, 0), (0, u_{\partial T})) \\ &= \mathbf{a}_T((0, u_{\partial T}), (0, u_{\partial T})) - \mathbf{a}_T((\mathcal{S}_T u_{\partial T}, 0), (\mathcal{S}_T u_{\partial T}, 0)), \\ &\leq \mathbf{a}_T((0, u_{\partial T}), (0, u_{\partial T})) \end{aligned}$$

where the second line follows from equation (2.15) with $v_T = \mathcal{S}_T u_{\partial T}$ and the symmetry of \mathbf{a}_T , and the conclusion from the fact that \mathbf{a}_T is semi-definite positive. Therefore, by equations (2.10) and (3.5),

$$\mathbf{a}_T((\mathcal{S}_T u_{\partial T}, u_{\partial T}), (0, u_{\partial T})) \lesssim (k+1)^2 h_T^{-1} \|u_{\partial T}\|_{\partial T}^2. \quad (3.8)$$

Thus, combining (3.7) and (3.8) it holds that

$$\sum_{T \in \mathcal{T}_h} h_T \|u_{\partial T}\|_{\partial T}^2 \lesssim A_h(u_{\mathcal{F}_h}, u_{\mathcal{F}_h}) \lesssim (k+1)^2 \sum_{T \in \mathcal{T}_h} h_T^{-1} \|u_{\partial T}\|_{\partial T}^2.$$

Gathering by faces (and recalling that $u_{\mathcal{F}_h}$ vanishes on boundary faces), we obtain

$$\sum_{F \in \mathcal{F}_h^i} (h_{T_F^+} + h_{T_F^-}) \|u_F\|_F^2 \lesssim A_h(u_{\mathcal{F}_h}, u_{\mathcal{F}_h}) \lesssim (k+1)^2 \sum_{F \in \mathcal{F}_h^i} (h_{T_F^+}^{-1} + h_{T_F^-}^{-1}) \|u_F\|_F^2. \quad (3.9)$$

Having chosen orthonormal bases on the space $\mathbb{P}^k(F)$, and recalling the definitions of $H_{\mathcal{F}_h, \min}$ and $H_{\mathcal{F}_h, \max}$, this relation reduces to

$$H_{\mathcal{F}_h, \min} \mathbf{U} \cdot \mathbf{U} \lesssim \mathbf{A}_h \mathbf{U} \cdot \mathbf{U} \lesssim (k+1)^2 H_{\mathcal{F}_h, \max}^{-1} \mathbf{U} \cdot \mathbf{U}. \quad (3.10)$$

The estimates (2.19) classically follow from these bounds. \square

Remark 3 (Non-orthonormal polynomial bases). *The choice of orthonormal bases allows us, in the proof above, to substitute each $\|u_F\|_F^2$ in (3.9) with the Euclidean norm of the coefficients of u_F on the basis of $\mathbb{P}^k(F)$, thus leading to the global expressions $H_{\mathcal{F}_h, \min} \mathbf{U} \cdot \mathbf{U}$ and $H_{\mathcal{F}_h, \max}^{-1} \mathbf{U} \cdot \mathbf{U}$ in (3.10). If non-orthonormal polynomial bases are chosen in some $\mathbb{P}^k(F)$, the proof shows that $H_{\mathcal{F}_h, \min}$ and $H_{\mathcal{F}_h, \max}$ have to be adjusted the following way: for each F , letting c_F, C_F be positive constants such that, for the chosen basis $(q_i^F)_{i \in I_F}$ of $\mathbb{P}^k(F)$, we have*

$$c_F \sum_{i \in I_F} \lambda_i^2 \leq \left\| \sum_{i \in I_F} \lambda_i q_i^F \right\|_F^2 \leq C_F \sum_{i \in I_F} \lambda_i^2 \quad \forall (\lambda_i)_{i \in I_F} \in \mathbb{R},$$

we set

$$H_{\mathcal{F}_h, \min} = \min_{F \in \mathcal{F}_h} c_F \left(h_{T_F^+} + h_{T_F^-} \right), \quad H_{\mathcal{F}_h, \max}^{-1} = \max_{F \in \mathcal{F}_h} C_F \left(h_{T_F^+}^{-1} + h_{T_F^-}^{-1} \right).$$

It should be noted that c_F and C_F might depend, for some choice of polynomial bases, on the face geometry and its size. In this case, the resulting estimates on the eigenvalues and condition number may not be robust with respect to small faces in the mesh, on the contrary to those obtained using orthonormal bases (the importance, for meshes containing distorted elements, of using orthonormal bases over, say, monomial bases was already noticed in [18, Section B.1]).

3.2 Analysis of the stabilisation

We prove here the validity of the stabilisation term s_T defined by (2.11), and provide a brief discussion of alternate choices of stabilisation bilinear form. As the coercivity and boundedness (2.7), and polynomial consistency (2.8) are well established for the stabilisations considered here, we only wish to show that Assumption 2 holds true.

Lemma 6. *The stabilisation bilinear form defined by (2.11) satisfies Assumption 2.*

Proof. The lower bound (2.9) follows trivially by noting that for all $\underline{v}_T \in \underline{U}_T^{k,l}$, we have

$$a_T(\underline{v}_T, \underline{v}_T) = \|\nabla \mathbf{p}_T^{k+1} \underline{v}_T\|_T^2 + h_T^{-2} \|\delta_T^l \underline{v}_T\|_T^2 + h_T^{-1} \|\delta_{\partial T}^k \underline{v}_T\|_{\partial T}^2.$$

To prove the bound (2.10) it remains to show that, for all $\underline{v}_{T,\partial} = (0, v_{\partial T}) \in \underline{U}_T^{k,l}$,

$$h_T^{-2} \|\delta_T^l \underline{v}_{T,\partial}\|_T^2 \lesssim \|\nabla \mathbf{p}_T^{k+1} \underline{v}_{T,\partial}\|_T^2 + h_T^{-1} \|\delta_{\partial T}^k \underline{v}_{T,\partial}\|_{\partial T}^2.$$

We invoke the boundedness of $\pi_T^{0,l}$ and the Poincaré–Wirtinger (3.3) inequality, valid since $\pi_T^{0,0} \mathbf{p}_T^{k+1} \underline{v}_{T,\partial} = 0$ by (2.6), to see that

$$h_T^{-2} \|\delta_T^l \underline{v}_{T,\partial}\|_T^2 = h_T^{-2} \|\pi_T^{0,l} \mathbf{p}_T^{k+1} \underline{v}_{T,\partial}\|_T^2 \leq h_T^{-2} \|\mathbf{p}_T^{k+1} \underline{v}_{T,\partial}\|_T^2 \lesssim \|\nabla \mathbf{p}_T^{k+1} \underline{v}_{T,\partial}\|_T^2,$$

thus, completing the proof. \square

3.2.1 Alternate choices for the stabilisation bilinear form

We briefly comment here on a variety of different choices for the stabilisation term s_T . For the choice of element polynomial degree $l = k - 1$, the stabilisation bilinear form $s_T^{(k-1)} : \underline{U}_T^{k-1,k} \times \underline{U}_T^{k-1,k} \rightarrow \mathbb{R}$ defined for all $\underline{v}_T, \underline{w}_T \in \underline{U}_T^{k-1,k}$ via

$$s_T^{(k-1)}(\underline{v}_T, \underline{w}_T) := h_T^{-1} (\delta_{\partial T}^k \underline{v}_T, \delta_{\partial T}^k \underline{w}_T)_{\partial T}$$

satisfies the requirements (2.7) and (2.8) [23, Section 4.3]. Moreover, it is clear that $s_T^{(k-1)}$ satisfies Assumption 2 with hidden constant in (2.9) and (2.10) equal to 1. We emphasise, however, that when $l > k - 1$ the coercivity (2.7) of a_h fails for this choice of stabilisation, and that the discrete problem (2.13) is ill posed.

Another choice of stabilisation with only boundary terms is the “original HHO stabilisation” $s_T^\partial : \underline{U}_T^{l,k} \times \underline{U}_T^{l,k} \rightarrow \mathbb{R}$ defined for all $\underline{v}_T, \underline{w}_T \in \underline{U}_T^{l,k}$ via

$$s_T^\partial(\underline{v}_T, \underline{w}_T) := h_T^{-1} ((\delta_{\partial T}^k - \delta_T^l) \underline{v}_T, (\delta_{\partial T}^k - \delta_T^l) \underline{w}_T)_{\partial T}. \quad (3.11)$$

It satisfies the coercivity and boundedness requirements (2.7) for all $l \leq k + 1$ [18, Proposition 2.13]. This choice of stabilisation also satisfies the upper bound (2.10) in Assumption 2, however, we have been yet unable to prove the lower bound (2.9) with a constant that does not depend on k .

Remark 4 (HDG stabilisation). *In the case $l = k + 1$, the following HDG-inspired stabilisation can also be considered (see [18, Section 5.1.6] and [14]):*

$$s_T^{\text{HDG}}(\underline{v}_T, \underline{w}_T) = h_T^{-1} (\pi_{\partial T}^{0,k} (v_{\partial T} - v_T), \pi_{\partial T}^{0,k} (w_{\partial T} - w_T))_{\partial T}.$$

As for s_T^∂ above, we can prove a uniform-in- k upper bound (2.10) for s_T^{HDG} , but the lower bounds we could establish depend on k .

The gradient-based stabilisation $s_T^\nabla : \underline{U}_T^{l,k} \times \underline{U}_T^{l,k} \rightarrow \mathbb{R}$ introduced in [23, Section 4] is defined for all $\underline{v}_T, \underline{w}_T \in \underline{U}_T^{l,k}$ via

$$s_T^\nabla(\underline{v}_T, \underline{w}_T) := (\nabla \delta_T^l \underline{v}_T, \nabla \delta_T^l \underline{w}_T)_T + h_T^{-1} (\delta_{\partial T}^k \underline{v}_T, \delta_{\partial T}^k \underline{w}_T)_{\partial T}. \quad (3.12)$$

The gradient-based stabilisation satisfies coercivity, boundedness, and polynomial consistency for all $l \geq k-1$. Moreover, it is clear that s_T^∇ satisfies equation (2.9) in Assumption 2. For $l \geq k+1$, the upper bound (2.10) also follows trivially. However, for $l = k-1, k$ we have been unable to prove that this choice of stabilisation satisfies (2.10) without an extra dependency on k .

Despite these shortcomings in the analysis, numerical tests suggest that s_T^∂ and s_T^∇ satisfy the eigenvalue estimates stated in Theorem 1. This is illustrated in Figure 3. Moreover, these choices of stabilisation might be preferable as the error induced when measured in certain norms can be significantly lower than for the choice (2.11) [23, Figures 2, 3].

4 HHO on cut meshes

As discussed in the introduction, the generation of unstructured body-fitted meshes of geometrically complex regions – such as those with curved boundaries and high curvatures – can present great difficulties. Unfitted finite element methods avoid this issue because they are defined on a simple (e.g., Cartesian or octree) background mesh covering the domain of interest. The elements in touch with interface boundaries can be locally cut to produce polytopal elements on the physical domain boundaries [2]. These cuts can produce narrow, anisotropic ‘sliver-cut’ elements, as well as small but round ‘small-cut’ elements.

The design of a variant of the HHO method on cut meshes, with potentially curved elements, is presented and analysed in [10] for elliptic interface problems. The unfitted HHO method therein makes use of Nitsche’s method for the local reconstruction operator. Instead, we consider a standard HHO method on cut meshes. In particular, we define a simple structured background mesh $\mathcal{T}_h^{\text{bg}}$ and extract the submesh of active elements $\mathcal{T}_h^{\text{act}}$. The active mesh is split into interior elements $\mathcal{T}_h^{\text{in}}$ and cut elements $\mathcal{T}_h^{\text{cut}}$.

Based on the condition number bounds in Theorem 1, we know that the conditioning of the system matrix can be severely affected by the presence of small-cut and sliver-cut elements. To attain condition number bounds on cut meshes that are independent of the cut location, sliver-cut and small-cut elements in $\mathcal{T}_h^{\text{cut}}$ are aggregated to their neighbours to form an isotropic, quasi-uniform mesh. In particular, we iterate over elements $T \in \mathcal{T}_h^{\text{cut}}$ and merge T with its neighbour sharing the longest edge (or face) if

$$\frac{|T|_d}{|\partial T|_{d-1}} < \epsilon_1 h_T \quad \text{or} \quad h_T < \epsilon_2 h_{\max}.$$

The algorithm is re-run until no ill-posed elements are found. The convergence of this algorithm is assured, since any ill-posed cell is at finite distance to a well-posed cell. The size of the aggregates is bounded by the maximum of such distance for all ill-cells, which depends on the scale of the geometrical features (see [5, Lemma 2.2]). We take $\epsilon_1 = 0.05$ and $\epsilon_2 = 0.3$ in the numerical experiments section. After this aggregation step, we end up with a new mesh $\mathcal{T}_h^{\text{ag}}$. Let us note that arbitrarily small faces can still be present in $\mathcal{T}_h^{\text{ag}}$. The following corollary is a direct consequence of Theorem 1 and the aggregation algorithm.

Corollary 7 (Eigenvalues and condition numbers on cut meshes). *Let $\mathcal{T}_h^{\text{bg}}$ be a background mesh covering Ω with characteristic mesh size h and $\mathcal{T}_h^{\text{ag}}$ the corresponding aggregated mesh obtained*

using the algorithm described above. Let \mathbf{A}_h be the linear system matrix corresponding to the HHO discretisation (2.17) for $\mathcal{T}_h^{\text{ag}}$. Under the assumptions in Theorem 1, it holds:

$$\lambda_{\min}(\mathbf{A}_h) \gtrsim h, \quad \lambda_{\max}(\mathbf{A}_h) \lesssim (k+1)^2 h^{-1}, \quad \kappa(\mathbf{A}_h) \lesssim (k+1)^2 h^{-2},$$

where the constants are independent of the cut location but depend on the choice of ϵ_1 and ϵ_2 .

We note that the ill-conditioning of systems arising in unfitted C^0 -Lagrangian FEs can be solved by aggregating ill-conditioned elements into their neighbours [5]. However, the strategy we consider here is simpler because there is no need to eliminate ill-posed nodes via constraints in each aggregate.

5 Numerical Results

We provide here a numerical study of the condition number to illustrate the results derived in previous sections. The linear system (2.17) is assembled using the **HArDCore** open source C++ library [21]. We compute the condition number using the **SymEigsSolver** solver found in the **Spectra** library, with documentation available at <https://spectralib.org/doc/index.html>. All numerical tests in this section are performed using element degree $l = k$, and L^2 -orthonormalised basis functions. The orthonormalisation process is achieved using a classical Gram-Schmidt algorithm.

5.1 Coarsened meshes

In order to capture intricate geometric details in a given domain it is sometimes sensible to start with a regular, fine mesh of small element diameter, and agglomerate elements together in order to save computation time. These coarsened meshes are (relatively) isotropic and quasi-uniform, however can have many faces per element and arbitrarily small face diameters. Thus, Theorem 1 predicts the maximum and minimum eigenvalues to scale as $\lambda_{\min}(\mathbf{A}_h) \approx h$ and $\lambda_{\max}(\mathbf{A}_h) \approx h^{-1}$ respectively, independently of the number and size of faces in each element. We consider the unit box $\Omega = (0, 1)^2 \subset \mathbb{R}^2$, and a fine triangular mesh of Ω . We then design successive coarsenings of these meshes and observe how the condition number evolves. Such meshes are plotted in Figure 1 with the data of the mesh sequence presented in Table 1.

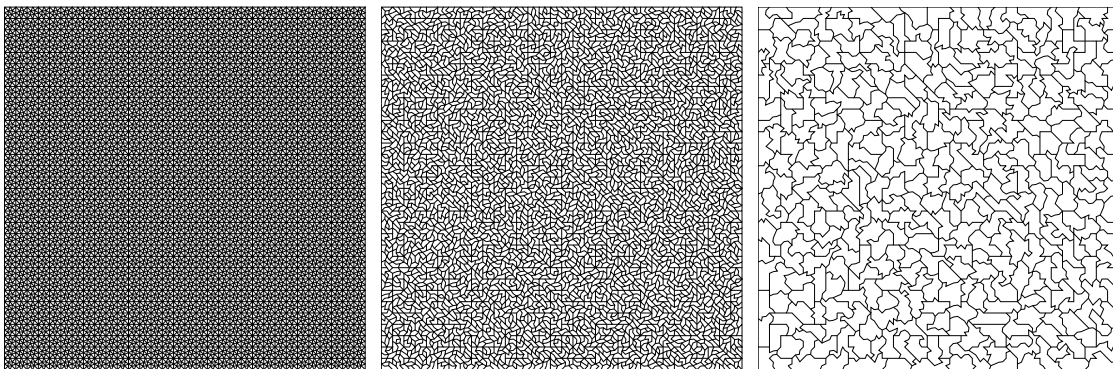


Figure 1: Coarsened meshes

h_{\min}	h_{\max}	Nb. Elements	Nb. Internal Edges
$1.19 \cdot 10^{-2}$	$1.56 \cdot 10^{-2}$	14,336	21,376
$1.19 \cdot 10^{-2}$	$2.38 \cdot 10^{-2}$	8,066	15,106
$1.56 \cdot 10^{-2}$	$3.49 \cdot 10^{-2}$	4,440	11,480
$2.21 \cdot 10^{-2}$	$6.25 \cdot 10^{-2}$	2,390	8,783
$2.87 \cdot 10^{-2}$	$8.47 \cdot 10^{-2}$	1,285	6,510
$3.76 \cdot 10^{-2}$	0.11	684	4,825
$6.11 \cdot 10^{-2}$	0.13	363	3,633
$7.51 \cdot 10^{-2}$	0.19	193	2,708
0.11	0.24	103	2,020
0.14	0.33	56	1,488
0.24	0.49	29	1,056

Table 1: Coarsened meshes

The condition number and eigenvalues on each mesh are plotted in Figure 2. As the mesh is coarsened the condition number appears to decay slightly slower than h^{-2} . This is easily explainable due to the successive meshes becoming less ‘round’, and thus the mesh regularity parameter increasing slightly with each level of coarsening.

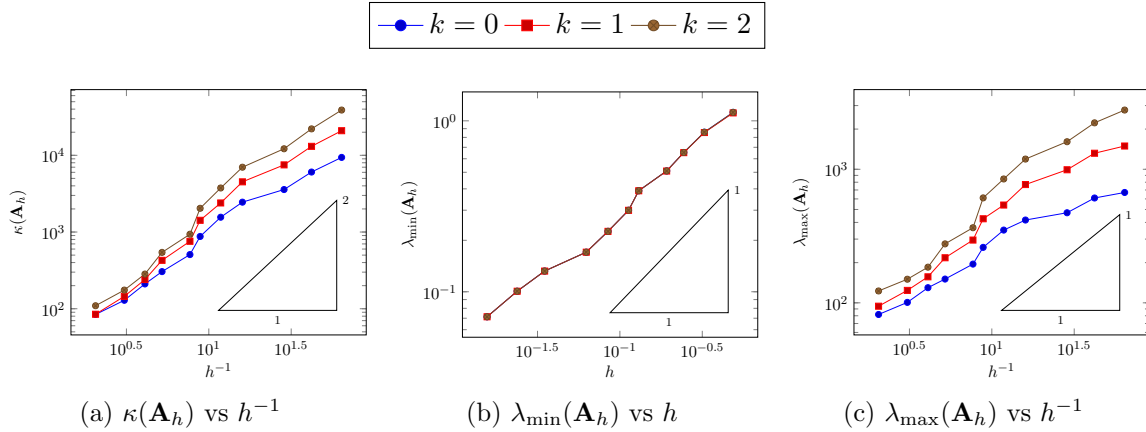


Figure 2: Coarse square meshes

In Figure 3 we fix the mesh (the mesh with $h_{\min} = 0.11$ in Table 1) and vary the polynomial degree k . We test with the stabilisation defined by (2.11) as well as the gradient-based (3.12) and boundary (3.11) stabilisations. It is apparent from Figure 3 that all three stabilisations result in a system matrix with eigenvalue estimates determined by Theorem 1.

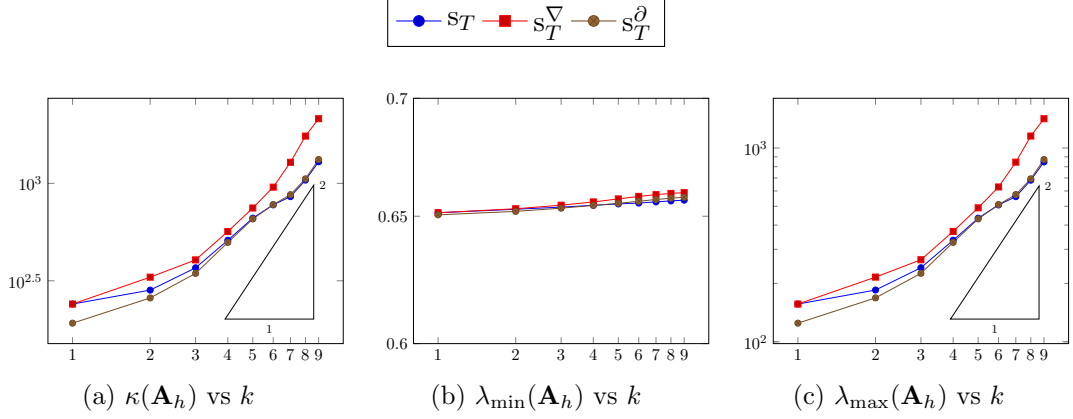


Figure 3: Condition number vs polynomial degree

5.2 Cut meshes

In this section, we apply the HHO method to cut meshes using the aggregation strategy proposed above. The computation of the cut meshes and the boundary-element intersections has been carried out using the `Gridap` open-source Julia library [4] version 0.16.3 and its extension package for unfitted methods `GridapEmbedded.jl` [30] version 0.7 (see [2] for more details). We consider first-order boundary representations – that is, we consider a piecewise linear approximation of the curved boundary.

5.2.1 Test A

Take the circular domain $\Omega = \{(x, y) \in \mathbb{R}^2 : x^2 + y^2 < 1\} \subset \mathbb{R}^2$ and consider three similar cut meshes of Ω , with a parameter ϵ controlling the diameter of the smallest cut elements ($\epsilon < h_T$ for all $T \in \mathcal{T}_h$). The mesh data is given in Table 2, and we plot values of the condition number and eigenvalues versus ϵ in Figure 4. It is clear that both the maximum eigenvalue, and the condition number, become unbounded as $\epsilon \rightarrow 0$. The minimum eigenvalue, however, stays approximately constant. This is consistent with the theory as each face is connected to at least one element with diameter proportional to h_{\max} , thus we expect $\lambda_{\min}(\mathbf{A}_h) \sim h_{\max} = \text{const.}$

ϵ	h_{\min}	h_{\max}	Nb. Elements	Nb. Internal Edges
$1 \cdot 10^{-2}$	$1.14 \cdot 10^{-2}$	0.28	154	202
$1 \cdot 10^{-3}$	$1.13 \cdot 10^{-3}$	0.28	154	202
$1 \cdot 10^{-4}$	$1.13 \cdot 10^{-4}$	0.28	154	202

Table 2: Parameters of the circular meshes with varying values of ϵ

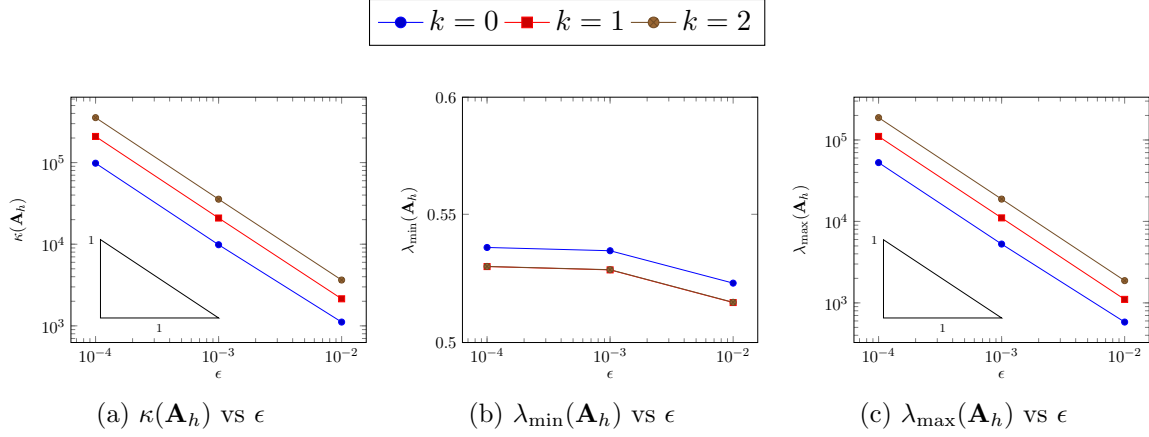


Figure 4: Cut meshes with small-cut elements

To avoid unbounded condition numbers on cut meshes, sliver and small-cut elements are aggregated as explained above. A portion of the resulting aggregated mesh $\mathcal{T}_h^{\text{ag}}$ of Ω is plotted in Figure 5 showing the aggregation of sliver-cut and small-cut elements. We note the existence of arbitrarily small faces after the aggregation of small-cut elements.

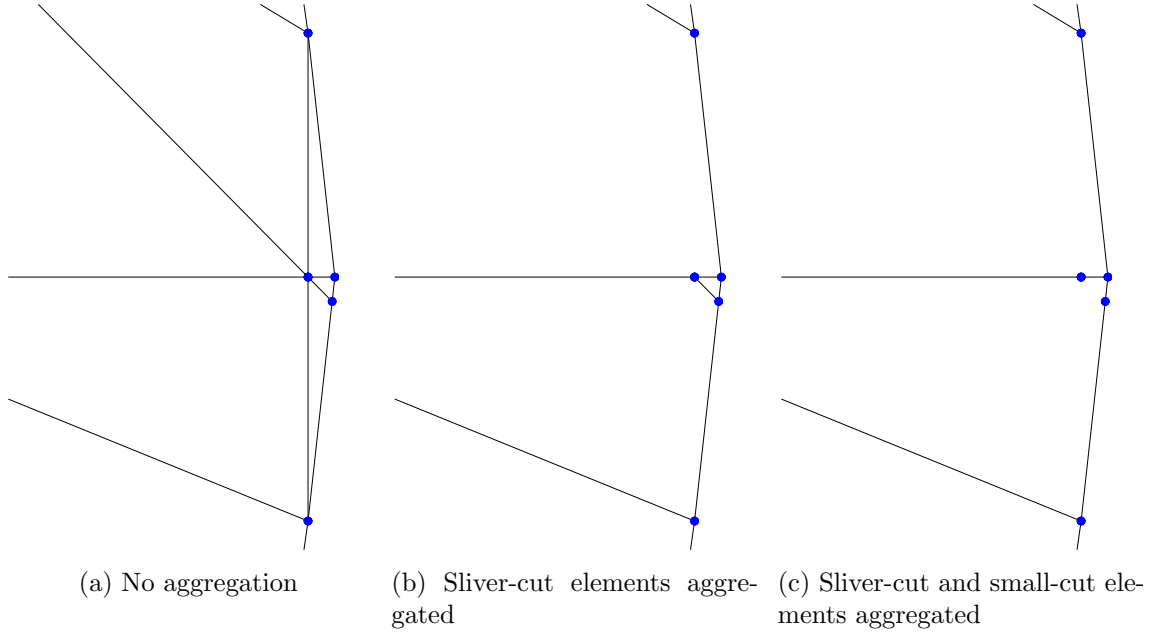


Figure 5: Aggregation of cut meshes (local)

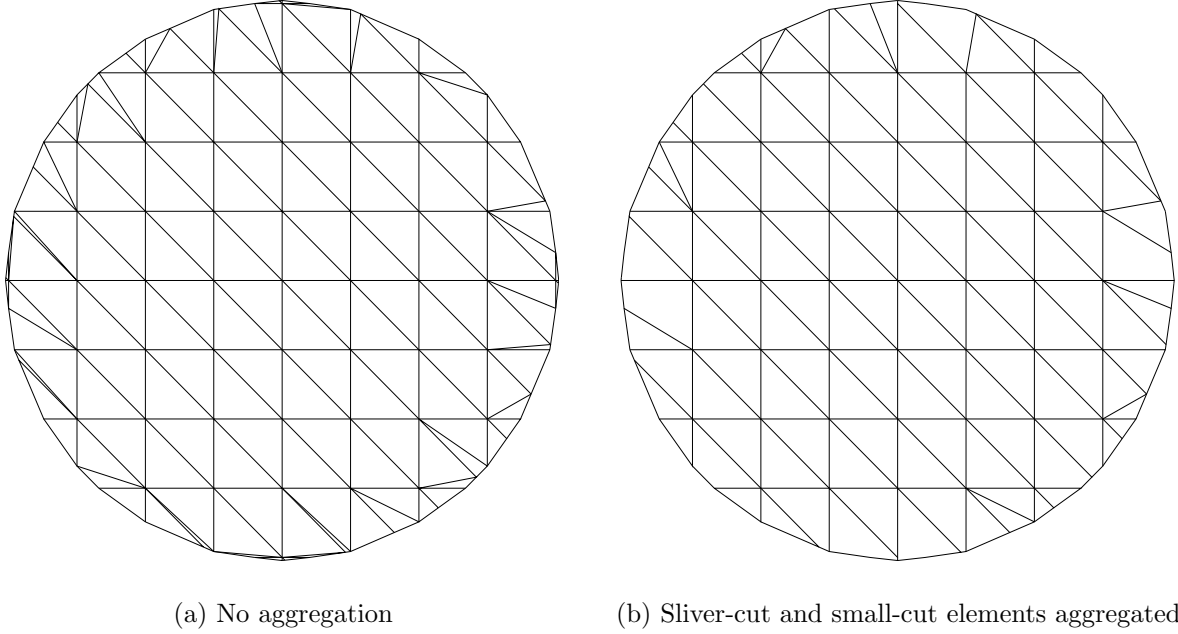


Figure 6: Aggregation of cut meshes (global)

For each mesh in Table 2 we consider a corresponding aggregated mesh, and in Figure 7 we test the condition number and eigenvalues of the system matrix for various polynomial degrees k . It is clear that after aggregation the minimal eigenvalue, maximal eigenvalue and condition number are independent of ϵ .

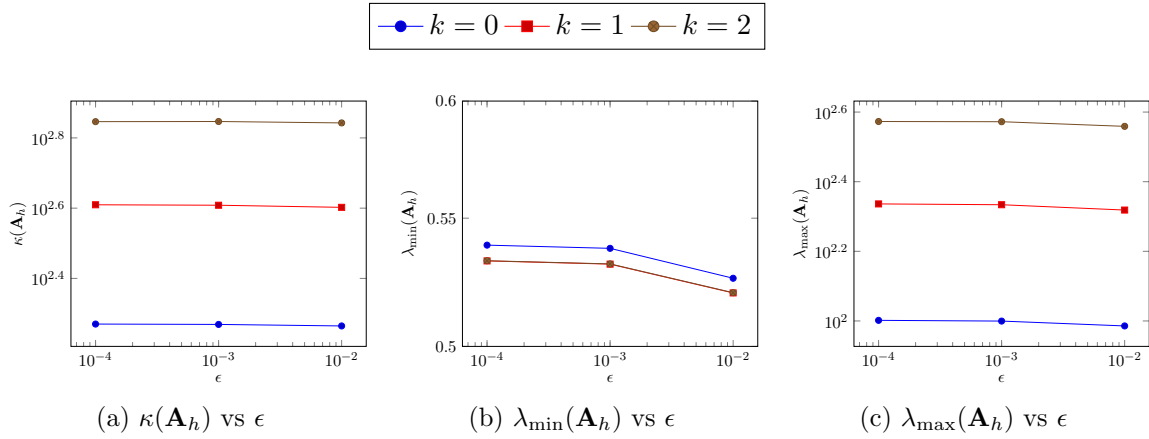


Figure 7: Cut meshes with aggregated elements

5.2.2 Test B

We now consider a sequence of cut and approximate meshes of the circular domain $\Omega = \{(x, y) \in \mathbb{R}^2 : x^2 + y^2 < 1\}$ and track the conditioning of the scheme before and after the agglomeration of sliver-cut and small-cut elements. The parameters of this sequence of meshes are given in Table 3 and three of the meshes are plotted in Figure 8.

h_{\min}	h_{\max}	Nb. Elements	Nb. Internal Edges
0.16	0.57	48	59
$1.14 \cdot 10^{-2}$	0.28	154	202
$4.07 \cdot 10^{-3}$	0.14	538	750
$4.7 \cdot 10^{-3}$	$9.43 \cdot 10^{-2}$	1,098	1,562
$2.32 \cdot 10^{-3}$	$7.07 \cdot 10^{-2}$	1,878	2,706

Table 3: Parameters of the meshes used in Test B prior to aggregation

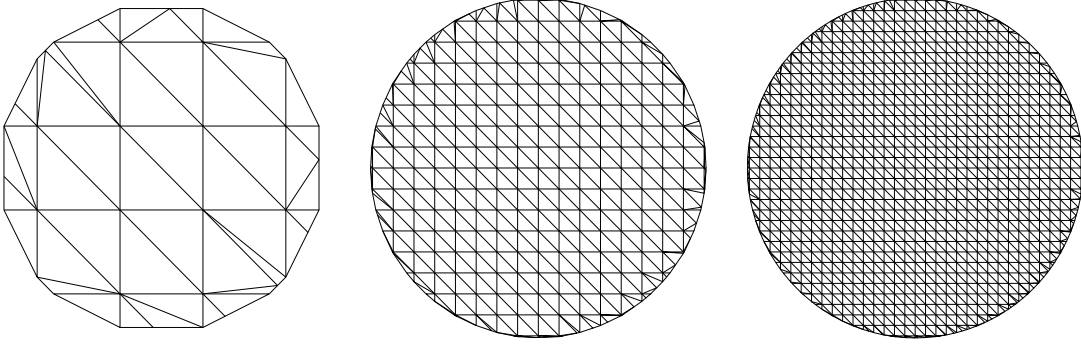


Figure 8: Three of the meshes used in Test B prior to aggregation

Prior to aggregation of small-cut elements, each face is attached to at least one element of diameter proportional to h_{\max} . Thus we expect to observe $\lambda_{\min}(\mathbf{A}_h) \sim h_{\max}$ and $\lambda_{\max}(\mathbf{A}_h) \sim h_{\min}^{-1}$. In Figure 9 we plot the condition number and eigenvalues for each mesh prior to aggregation. The results are not smooth due to the presence of sliver-cut elements which have potentially very large mesh regularity parameters. In Figure 10, we observe that after the agglomeration of sliver-cut elements the results behave as predicted by theory.

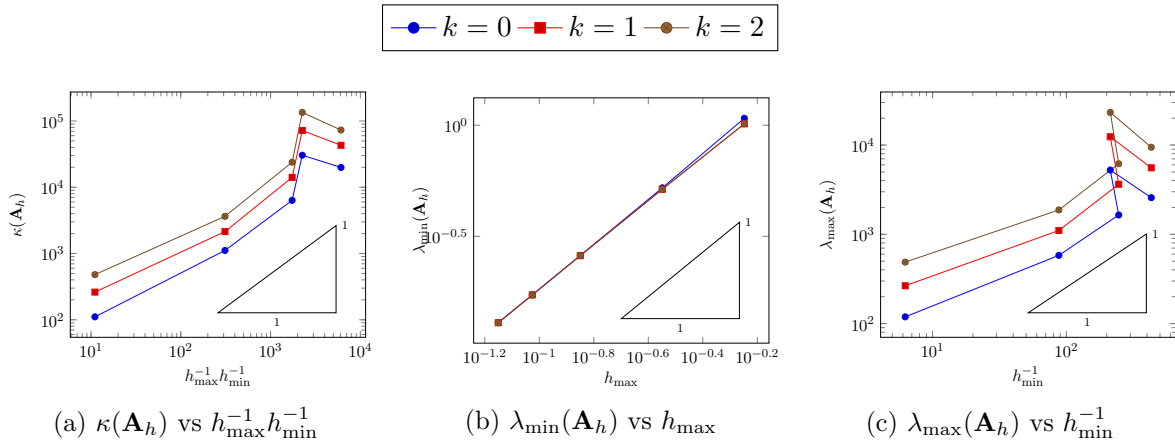


Figure 9: Circular meshes with no aggregation

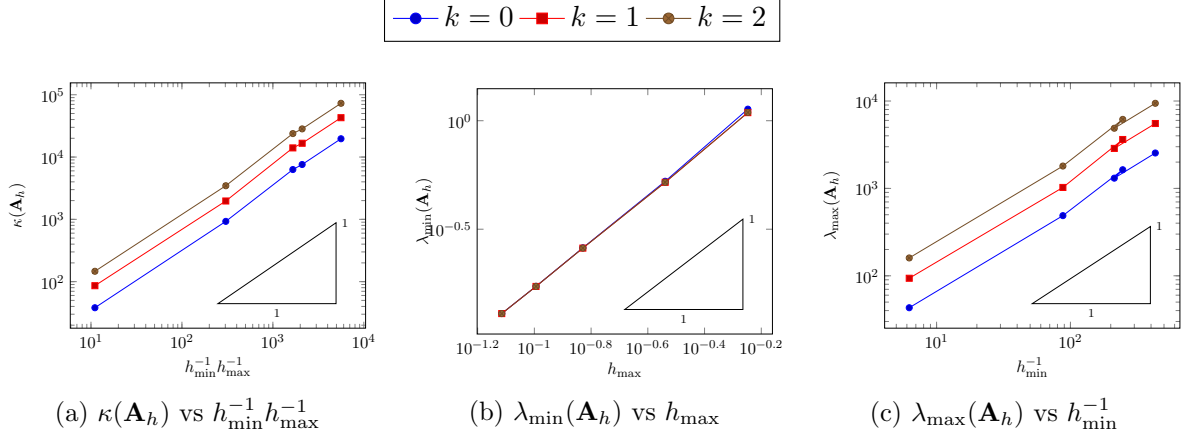


Figure 10: Circular meshes with sliver-cut elements aggregated

In Figure 11, results are plotted with both sliver-cut and small-cut elements aggregated. The condition number is one order of magnitude smaller than it was prior to aggregation, and scales as h^{-2} . Again, this is expected due to the meshes being quasi-uniform ($h = h_{\max} \sim h_{\min}$).

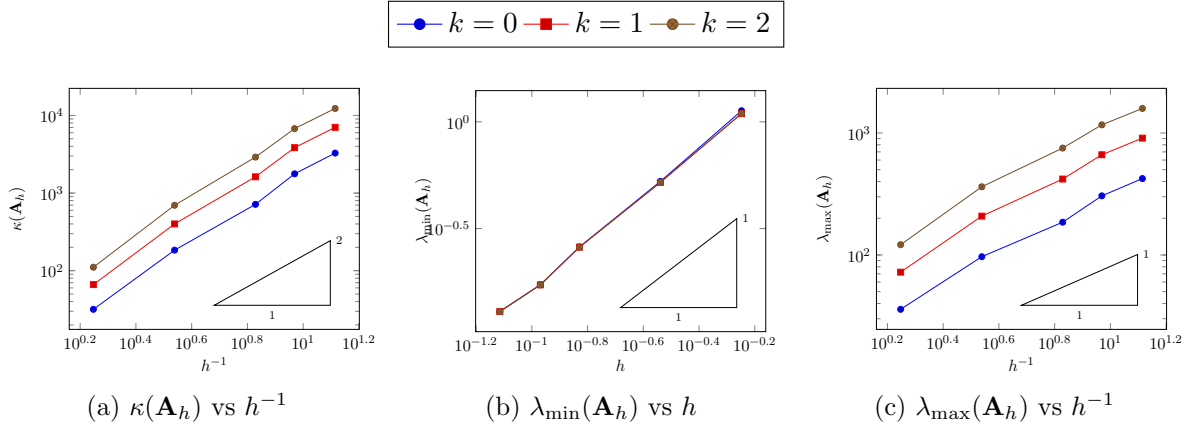


Figure 11: Circular meshes with sliver-cut and small-cut elements aggregated

5.3 Penta-diagonal meshes

We consider in this section a family of meshes with a penta-diagonal of elements being refined, and two large elements on each side (see Figure 12). The purpose of this test is to assess the accuracy of our estimates, and the robustness of the HHO condition number itself, when some large elements are neighbouring very small elements, all the while having an increasing number of faces. While testing on such extreme meshes is possibly contrived, the behaviour of the condition number illustrates that in some situations the estimates of Theorem 1 can be improved.

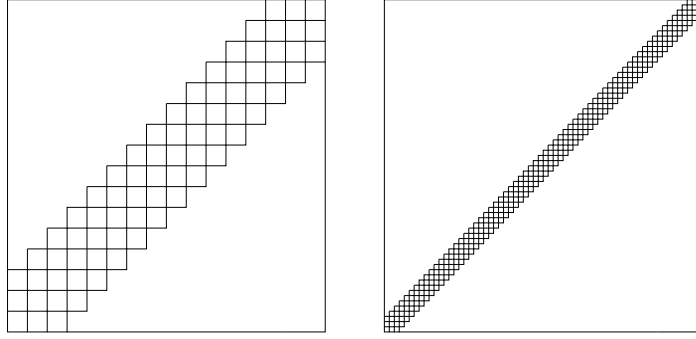


Figure 12: Penta-diagonal square meshes

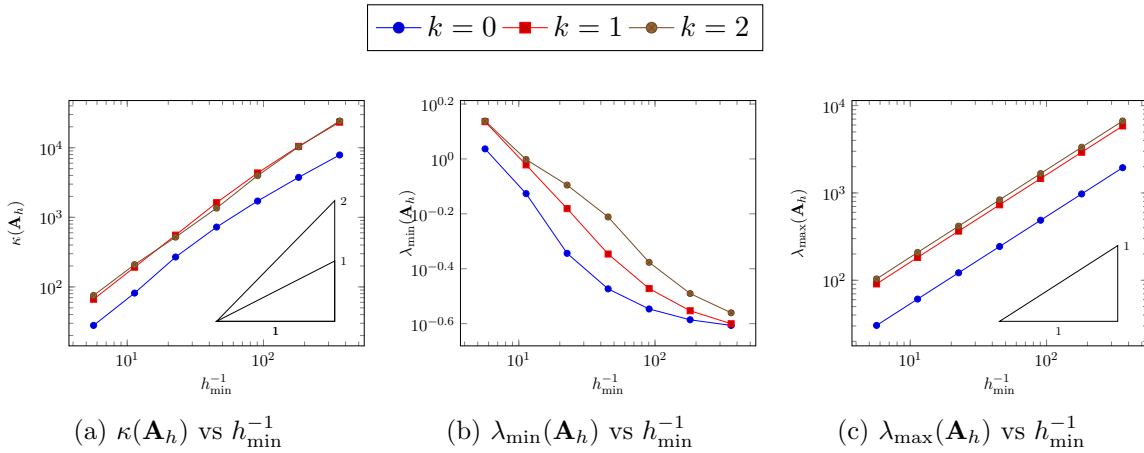


Figure 13: Penta-diagonal square meshes

The results presented in Figure 13 show a growth of the maximum eigenvalue as $\mathcal{O}(h_{\min}^{-1})$, which is consistent with the estimate (2.19b). Figure 13b however seems to indicate that, for this family of meshes, $\lambda_{\min}(\mathbf{A}_h)$ actually remains bounded below, which would indicate that the estimate (2.19a) is not optimal; it can actually be proved (see Lemma 8) that for these meshes the minimal eigenvalue indeed remains bounded below. As a consequence, the condition number $\kappa(\mathbf{A}_h)$ does not grow as $\mathcal{O}(h_{\min}^{-2})$ but as $\mathcal{O}(h_{\min}^{-1})$, which is illustrated in Figure 13a.

Lemma 8. *For the family of penta-diagonal meshes, it holds that $\lambda_{\min}(\mathbf{A}_h) \gtrsim 1$.*

Proof. We first note that even if the penta-diagonal meshes do not satisfy Assumption 1 (due to the two large elements with “stairs” boundary), the analysis carried out in the previous sections still applies. Indeed, we can easily find uniform bi-Lipschitz mappings between each of these elements and a ball of size comparable to these elements, which ensures that the trace inequality (3.1) still holds; since all elements contain a ball of size comparable to their diameters, the other relevant inequalities (approximation properties of projectors, discrete inverse inequalities) also remain valid.

An inspection of the proof of Theorem 1 (see in particular (3.7)) reveals that the bound on $\lambda_{\min}(\mathbf{A}_h)$ is a direct consequence of (3.4). The result thus follows if we establish this improved version of (3.4), in which the scaling factor h_T has been removed from the left-hand side: for all

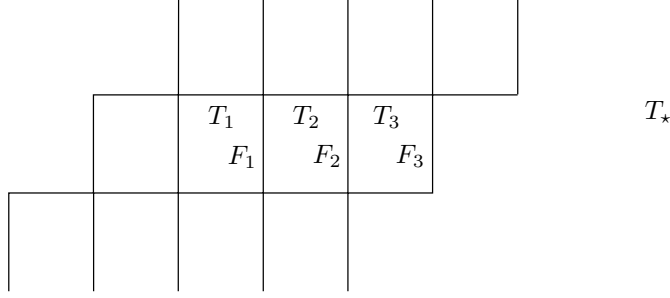


Figure 14: Illustration of the proof of Lemma 8.

$$\underline{v}_h \in \underline{U}_{h,0}^{k,l},$$

$$\sum_{T \in \mathcal{T}_h} \|v_{\partial T}\|_{\partial T}^2 \lesssim \sum_{T \in \mathcal{T}_h} \left(\|\nabla p_T^{k+1} \underline{v}_T\|_T^2 + h_T^{-1} \|\delta_{\partial T}^k \underline{v}_T\|_{\partial T}^2 \right). \quad (5.1)$$

Let us take a face F in one of the small elements. Assuming for example that F is a vertical face, we can create a finite sequence of vertical faces ($F = F_1, F_2, \dots, F_r$) (with $r \leq 3$) such that F_r is a face of one of the two big elements in the mesh, say T_* ; see Figure 14 for an illustration.

Denoting by $(T_1, \dots, T_r, T_{r+1} = T_*)$ the elements encountered along the sequence (F_1, \dots, F_r) , we can then write

$$\begin{aligned} \|v_F\|_F^2 &\leq \|v_{F_1} - \pi_{F_1}^{0,k} p_{T_2}^{k+1} \underline{v}_{T_2}\|_F^2 + \|p_{T_2}^{k+1} \underline{v}_{T_2} - \pi_{T_2}^{0,0} p_{T_2}^{k+1} \underline{v}_{T_2}\|_F^2 + \|\pi_{T_2}^{0,0} p_{T_2}^{k+1} \underline{v}_{T_2}\|_F^2 \\ &\lesssim \|\delta_{\partial T_2}^k \underline{v}_{T_2}\|_{\partial T_2}^2 + h_{T_2} \|\nabla p_{T_2}^{k+1} \underline{v}_{T_2}\|_{T_2}^2 + \|\pi_{T_2}^{0,0} p_{T_2}^{k+1} \underline{v}_{T_2}\|_{F_2}^2 \end{aligned} \quad (5.2)$$

where we have introduced $\pm \pi_{F_1}^{0,k} (p_{T_2}^{k+1} \underline{v}_{T_2} - \pi_{T_2}^{0,0} p_{T_2}^{k+1} \underline{v}_{T_2}) = \pm \pi_{F_1}^{0,k} p_{T_2}^{k+1} \underline{v}_{T_2} - \pi_{T_2}^{0,0} p_{T_2}^{k+1} \underline{v}_{T_2}$ and used the $L^2(F)$ -boundedness of $\pi_{F_1}^{0,k}$ and a triangle inequality in the first line, and invoked in the second line the bound $\|\delta_{F_1}^k \underline{v}_{T_2}\|_{F_1}^2 \leq \|\delta_{\partial T_2}^k \underline{v}_{T_2}\|_{\partial T_2}^2$, the continuous trace inequality (3.1) and Poincaré–Wirtinger inequality (3.3), and the fact that $\pi_{T_2}^{0,0} p_{T_2}^{k+1} \underline{v}_{T_2}$ is constant and $|F| = |F_2|$. By a similar argument it holds that

$$\begin{aligned} \|\pi_{T_2}^{0,0} p_{T_2}^{k+1} \underline{v}_{T_2}\|_{F_2}^2 &\leq \|\pi_{T_2}^{0,0} p_{T_2}^{k+1} \underline{v}_{T_2} - \pi_{F_2}^{0,k} p_{T_2}^{k+1} \underline{v}_{T_2}\|_{F_2}^2 + \|\pi_{F_2}^{0,k} p_{T_2}^{k+1} \underline{v}_{T_2} - v_{F_2}\|_{F_2}^2 + \|v_{F_2}\|_{F_2}^2 \\ &\lesssim h_{T_2} \|\nabla p_{T_2}^{k+1} \underline{v}_{T_2}\|_{T_2}^2 + \|\delta_{\partial T_2}^k \underline{v}_{T_2}\|_{\partial T_2}^2 + \|v_{F_2}\|_{F_2}^2. \end{aligned} \quad (5.3)$$

Thus, combining (5.2) and (5.3) we are able to write

$$\|v_{F_1}\|_{F_1}^2 \lesssim h_{T_2} \|\nabla p_{T_2}^{k+1} \underline{v}_{T_2}\|_{T_2}^2 + \|\delta_{\partial T_2}^k \underline{v}_{T_2}\|_{\partial T_2}^2 + \|v_{F_2}\|_{F_2}^2.$$

Iterating these estimates along the family (F_1, F_2, \dots, F_r) , using $r \leq 3$ and $h_{T_i} \lesssim 1$ we deduce that

$$\|v_F\|_F^2 \lesssim \sum_{i=2}^r \left(\|\nabla p_{T_i}^{k+1} \underline{v}_{T_i}\|_{T_i}^2 + h_{T_i}^{-1} \|\delta_{\partial T_i}^k \underline{v}_{T_i}\|_{\partial T_i}^2 \right) + \|v_{F_r}\|_{F_r}^2.$$

Summing this inequality over $F \in \mathcal{F}_T$ and then over the small elements T on the diagonal of the mesh, each of the small diagonal elements appear at most 3 times in the right-hand side, and the last boundary term is bounded above by $\|v_{\partial T_*}\|_{\partial T_*}^2$. This term can be estimated by introducing

$\pi_{\partial T_\star}^{0,k} \mathbf{p}_{T_\star}^{k+1} \underline{v}_{T_\star}$ as follows:

$$\begin{aligned} \|v_{\partial T_\star}\|_{\partial T_\star}^2 &\lesssim \|v_{\partial T_\star} - \pi_{\partial T_\star}^{0,k} \mathbf{p}_{T_\star}^{k+1} \underline{v}_{T_\star}\|_{\partial T_\star}^2 + \|\pi_{\partial T_\star}^{0,k} \mathbf{p}_{T_\star}^{k+1} \underline{v}_{T_\star}\|_{\partial T_\star}^2 \\ &\lesssim \|\delta_{\partial T_\star}^k \underline{v}_{T_\star}\|_{\partial T_\star}^2 + h_{T_\star} \|\nabla \mathbf{p}_{T_\star}^{k+1} \underline{v}_{T_\star}\|_{T_i}^2 + h_{T_\star}^{-1} \|\mathbf{p}_{T_\star}^{k+1} \underline{v}_{T_\star}\|_{T_\star}^2, \\ &\lesssim h_{T_\star}^{-1} \|\delta_{\partial T_\star}^k \underline{v}_{T_\star}\|_{\partial T_\star}^2 + \|\nabla \mathbf{p}_{T_\star}^{k+1} \underline{v}_{T_\star}\|_{T_i}^2 + \|\mathbf{p}_{T_\star}^{k+1} \underline{v}_{T_\star}\|_{T_\star}^2, \end{aligned}$$

where we have invoked the boundedness of $\pi_{\partial T_\star}^{0,k}$ and the continuous trace inequality (3.1), and in the final line we have used $h_{T_\star} \approx 1$, since T_\star is one of the large elements whose diameter does not go to zero. Combining all these estimates leads to

$$\sum_{T \in \mathcal{T}_h} \|v_{\partial T}\|_{\partial T}^2 \lesssim \sum_{T \in \mathcal{T}_h} \left(\|\nabla \mathbf{p}_T^{k+1} \underline{v}_T\|_T^2 + h_T^{-1} \|\delta_{\partial T}^k \underline{v}_T\|_{\partial T}^2 \right) + \|\mathbf{p}_h^{k+1} \underline{v}_h\|_{\Omega}^2.$$

The estimate (5.1) then follows in the same manner as in the proof of (3.4). \square

6 Conclusions

In this work, we prove detailed eigenvalue and condition number bounds for the linear system matrix that arises from HHO discretisations of the Laplace problem. The analysis applies to general polytopal meshes and polynomial orders. It reveals the effect of small and highly distorted elements and faces on the conditioning of the linear system. Whereas highly distorted elements negatively impact condition numbers, faces shapes and sizes do not affect these bounds. With this information, we apply HHO methods on cut meshes. We combine simple background meshes, element intersection algorithms and an aggregation strategy to end up with well-posed HHO methods on cut meshes.

We carry out a detailed set of numerical experiments that are in agreement with the numerical analysis. First, we analyse the condition number as one coarsens polytopal meshes with many faces per element and arbitrarily small faces. Next, we show that the HHO method on aggregated cut meshes provides the expected condition number with respect to the mesh size. We also observe that the condition number of the algorithm is not affected by increasingly small cut elements. Finally, we consider a limit case with penta-diagonal squared meshes that motivates sharper condition number bounds for some specific mesh configurations.

Future work includes the combination of HHO methods with higher-order cut geometrical discretisations (curved boundaries) and the design of optimal and scalable preconditioners for these linear systems.

Declarations

Funding This work was partially supported by the Australian Government through the *Australian Research Council's* Discovery Projects funding scheme (grant number DP210103092).

Competing Interests The corresponding author states on behalf of all authors, that there is no conflict of interest.

Code Availability All code used in this article is available in open source libraries and duly cited.

Data Availability The data generated in this article is available from the corresponding author on reasonable request.

References

- [1] Joubine Aghili, Daniele A Di Pietro, and Berardo Ruffini. An hp-hybrid high-order method for variable diffusion on general meshes. *Computational Methods in Applied Mathematics*, 17(3):359–376, 2017.
- [2] Santiago Badia, Pere A. Martorell, and Francesc Verdugo. Geometrical discretisations for unfitted finite elements on explicit boundary representations. *Journal of Computational Physics*, 460:111162, jul 2022.
- [3] Santiago Badia, Eric Neiva, and Francesc Verdugo. Linking ghost penalty and aggregated unfitted methods. *Computer Methods in Applied Mechanics and Engineering*, 388:114232, 2022.
- [4] Santiago Badia and Francesc Verdugo. Gridap: An extensible Finite Element toolbox in Julia. *Journal of Open Source Software*, 5(52):2520, 2020.
- [5] Santiago Badia, Francesc Verdugo, and Alberto F. Martín. The aggregated unfitted finite element method for elliptic problems. *Computer Methods in Applied Mechanics and Engineering*, 336:533–553, July 2018.
- [6] Laurenço Beirão da Veiga, Franco Brezzi, Andrea Cangiani, Gianmarco Manzini, L Donatella Marini, and Alessandro Russo. Basic principles of virtual element methods. *Mathematical Models and Methods in Applied Sciences*, 23(01):199–214, 2013.
- [7] Laurenço Beirão da Veiga, Claudio Canuto, Ricardo H Nochetto, and Giuseppe Vacca. Equilibrium analysis of an immersed rigid leaflet by the virtual element method. *Mathematical Models and Methods in Applied Sciences*, 31(07):1323–1372, 2021.
- [8] T Belytschko, N Moës, S Usui, and C Parimi. Arbitrary discontinuities in finite elements. *International Journal for Numerical Methods in Engineering*, 50(4):993–1013, 2001.
- [9] Erik Burman. Ghost penalty. *Comptes Rendus Mathématique*, 348(21-22):1217–1220, 2010.
- [10] Erik Burman, Matteo Cicuttin, Guillaume Delay, and Alexandre Ern. An unfitted hybrid high-order method with cell agglomeration for elliptic interface problems. *SIAM Journal on Scientific Computing*, 43(2):A859–A882, 2021.
- [11] Erik Burman, Susanne Claus, P Hansbo, M G Larson, and André Massing. CutFEM: Discretizing Geometry and Partial Differential Equations. *International Journal for Numerical Methods in Engineering*, 104(7):472–501, 2015.
- [12] Andrea Cangiani, Zhaonan Dong, Emmanuil H. Georgoulis, and Paul Houston. *hp-version discontinuous Galerkin methods on polygonal and polyhedral meshes*. SpringerBriefs in Mathematics. Springer, Cham, 2017.
- [13] Paul Castillo. Performance of discontinuous galerkin methods for elliptic pdes. *SIAM Journal on Scientific Computing*, 24(2):524–547, 2002.
- [14] B. Cockburn, D. A. Di Pietro, and A. Ern. Bridging the Hybrid High-Order and Hybridizable Discontinuous Galerkin methods. *ESAIM: Math. Model. Numer. Anal.*, 50(3):635–650, 2016.
- [15] B. Cockburn, O. Dubois, J. Gopalakrishnan, and S. Tan. Multigrid for an HDG method. *IMA Journal of Numerical Analysis*, 34(4):1386–1425, October 2013.

- [16] Bernardo Cockburn, Jayadeep Gopalakrishnan, and Raytcho Lazarov. Unified hybridization of discontinuous galerkin, mixed, and continuous galerkin methods for second order elliptic problems. *SIAM Journal on Numerical Analysis*, 47(2):1319–1365, January 2009.
- [17] F. de Prenter, C.V. Verhoosel, G.J. van Zwieten, and E.H. van Brummelen. Condition number analysis and preconditioning of the finite cell method. *Computer Methods in Applied Mechanics and Engineering*, 316:297–327, 2017. Special Issue on Isogeometric Analysis: Progress and Challenges.
- [18] Daniele Antonio Di Pietro and Jérôme Droniou. *The Hybrid High-Order Method for Polytopal Meshes: Design, Analysis, and Applications*, volume 19 of *Modeling, Simulation and Applications*. Springer International Publishing, <https://hal.archives-ouvertes.fr/hal-02151813>, 01 2020.
- [19] Daniele Antonio Di Pietro and Alexandre Ern. A hybrid high-order locking-free method for linear elasticity on general meshes. *Computer Methods in Applied Mechanics and Engineering*, 283:1–21, 2015.
- [20] Daniele Antonio Di Pietro, Alexandre Ern, and Simon Lemaire. An arbitrary-order and compact-stencil discretization of diffusion on general meshes based on local reconstruction operators. *Computational Methods in Applied Mathematics*, 14(4):461–472, 2014.
- [21] Jérôme Droniou. Hardcore.
- [22] Jérôme Droniou. Interplay between diffusion anisotropy and mesh skewness in hybrid high-order schemes. In *International Conference on Finite Volumes for Complex Applications*, pages 3–23. Springer, 2020.
- [23] Jérôme Droniou and Liam Yemm. Robust hybrid high-order method on polytopal meshes with small faces. *Comput. Methods Appl. Math.*, page 26p, 2021.
- [24] Alexandre Ern and Jean-Luc Guermond. Evaluation of the condition number in linear systems arising in finite element approximations. *ESAIM: Mathematical Modelling and Numerical Analysis*, 40(1):29–48, 2006.
- [25] Anita Hansbo and Peter Hansbo. An unfitted finite element method, based on Nitsche’s method, for elliptic interface problems. *Computer methods in applied mechanics and engineering*, 191(47-48):5537–5552, 2002.
- [26] August Johansson and Mats G. Larson. A high order discontinuous Galerkin Nitsche method for elliptic problems with fictitious boundary. *Numerische Mathematik*, 123(4):607–628, 2013.
- [27] Lorenzo Mascotto. Ill-conditioning in the virtual element method: Stabilizations and bases. *Numerical Methods for Partial Differential Equations*, 34(4):1258–1281, March 2018.
- [28] Eric Neiva and Santiago Badia. Robust and scalable h-adaptive aggregated unfitted finite elements for interface elliptic problems. *Computer Methods in Applied Mechanics and Engineering*, 380:113769, July 2021.
- [29] Dominik Schillinger and Martin Ruess. The Finite Cell Method: A review in the context of higher-order structural analysis of CAD and image-based geometric models. *Archives of Computational Methods in Engineering*, 22(3):391–455, 2015.

- [30] Francesc Verdugo, Eric Neiva, and Santiago Badia. GridapEmbedded. Version 0.7., October 2021. Available at <https://github.com/gridap/GridapEmbedded.jl>.